Applied Thermal Engineering 255 (2024) 124001

Contents lists available at ScienceDirect

Applied Thermal Engineering

journal homepage: www.elsevier.com/locate/apthermeng

Research Paper

A Rome district transition towards optimal and sustainable heat and power generation

Erfan Tajalli-Ardekani [a,*], Giovanni Delibra [b], Isabella Pizzuti [b], Alessandro Corsini [b]

[a] Dept. of Astronautical, Electrical and Energy Engineering, Sapienza University of Rome, Via Eudossiana 18, 00184 Roma, Italy
[b] Dept. of Mechanical and Aerospace Engineering, Sapienza University of Rome, Via Eudossiana 18, 00184 Roma, Italy

ARTICLE INFO

Keywords:
Urban district clean energy transition
Photovoltaic panels
Cogeneration and trigeneration
Battery energy storage
Multi-objective optimization
TRNSYS

ABSTRACT

In this work, a specific district of Rome energy metabolism has been studied to reduce the carbon footprint of electric and thermal energy generation. Two scenarios were investigated, one "*ex-ante*" with the district as it was, fully dependent on the national grid for electricity and methane-fuelled boilers for heating. And an "*ex-post*" scenario with the buildings retrofitted with more efficient thermal insulation, LED lights, photovoltaic panels and trigeneration systems. The energy metabolism of the district was modelled in TRNSYS in both cases. For the ex-post scenario, the digital twin implemented a control logic for energy flows with several functionalities including prioritizing the power flow, setting rules and boundaries on the operation of the co-generators, preventing batteries from overcharging/discharging. The sizing of PV panels, batteries, and cogeneration units in the ex-post scenario was optimized in terms of both energy and economic performance using a Python library with the Non-dominated Sorting Genetic algorithm (NSGA-II). In the ex-post scenario, the optimal energy system delivers significant reductions in energy costs and CO_2 emissions. The energy transition results in a decrease in purchased electricity of 68.2%, CO_2 emissions by 56% and generation costs by 48.9%. The Levelized Cost Of Energy (LCOE) of the district is estimated to be 196 €/MWh.

1. Introduction

Social, political and environmental and social background

The European Union (EU) has set the ambitious target to reduce greenhouse gas emissions by 55 % by 2030 [1]. To achieve this scope the increase of Renewable Energy Sources (RES) penetration counts as a key factor, as pointed out in [2]. In this context, many works detail the challenges and best practices from all over the EU. For example, Lund et al. [3] discuss best practices on district heating from Danish experiences with CHP (Combined Heat and Power), providing a roadmap to achieve carbon neutrality. Werner [4] reports on similar district heating experiences in Sweden, providing a thorough discussion on the energy market, the technical and supply context. He also discusses environmental and institutional issues of district heating, which in these experiences is strongly related to biomass and waste treatment. Buffa et al. [5] discuss further European experiences in Switzerland and Germany, focusing on the 5th generation technologies able to integrate electricity, heating and electric vehicles. Krajačić et al. [6] provide a thorough study of the clean energy transition in Croatia that involves several technologies with RES and respective storage systems. Starting with a 100 % RES planning, authors derived a solution that ends with a 78 % RES penetration, claiming that "to achieve a 100 % independent or a 100 % RES system, detailed planning of all economy sectors should be conducted" and in so doing points out the challenges related to achieving carbon–neutral conditions. Similar studies focus on Canadian experiences, e.g. in Ghorab [7], and Chinese district heating, e.g. Zhang et al. [8].

Technical challenges

Major technical challenges when dealing with the introduction of RES in urban districts are mostly related to the following issues, often with major interaction between each other:

- Electricity production, transmission and consumption
- Heating and cooling: production, transmission
- Integration of BESS and TESS in a system with increasing RES penetration
- Management of the smart district

There are several challenges due to the intermittent behavior of RES

* Corresponding author.
E-mail addresses: erfan.tajalliardekani@uniroma1.it (E. Tajalli-Ardekani), giovanni.delibra@uniroma1.it (G. Delibra), isabella.pizzuti@uniroma1.it (I. Pizzuti), alessandro.corsini@uniroma1.it (A. Corsini).

https://doi.org/10.1016/j.applthermaleng.2024.124001
Received 28 December 2023; Received in revised form 17 July 2024; Accepted 18 July 2024
Available online 19 July 2024

Nomenclature

Symbol

CAPEX	Capital Expenditure [€]
$Grid_{cb}$	Total Grid interaction cost/benefit [€]
NPV	Net Present Value [€]
LCOE	Levelized Cost Of Energy [€/*MWh*]
OPEX	O&M Expenditure [€]
PES	Primary energy saving index [%]
Pgrid	Grid power [*kW*]
PB	Payback period [*year*]
r	Discount rate [%]

Abbreviations

EMS	Energy Management System
HES	Hybrid Energy System
NSGA	Non-dominated Sorting Genetic Algorithm
OF	Objective Function
PV	Photovoltaic
RBC	Rule-Based Controller
RES	Renewable Energy Source
SoC	State of Charge

and the consequences on the electric grid, as pointed out by Abujarad et al. [9], that provide a review of unit commitment methods in power grids with intermittent RES, in particular discussing impacts of wind energy, PV solar and energy storage systems. Brouwer et al. [10] focus on modelling of these effects on different time scales (from seconds up to hours) and providing concurrent integration with thermal loads and production, addressing also curtailing in operations of the systems. Challenges related to voltage and frequency fluctuations are addressed in [11,12]. Vadi et al. [11] reviewed issues related to the control of these aspects in microgrids connected to the national grid, listing possible control strategies and optimization methods to reduce electrical losses. This aspect is further discussed in [12], where Wang et al. provide a specific study related to these effects in grids with a high photovoltaic production. Mohandes et al. [13] discuss the power system flexibility of grids with high penetration of renewables, highlighting the need for different types of reserves. These backups need to be characterized in terms of power capacity, ramping capacity and energy capacity to provide a complex enough mix of solutions.

Other issues related to Battery Energy Storage Systems (BESS) are discussed in Sun et al. [14], where the authors report on the latest advances in high-performance battery electrodes for flow batteries, focusing on the properties of electrospun carbon fibers as electrodes and their practical effects on different BESS. Diouf et al. [15] report on the increasing importance of lithium batteries and the challenges related to the industrial supply chain required to sustain massive implementation of BESS in smart grids.

Olatomiwa et al. [16] discussed energy management strategies in hybrid renewable energy systems, both grid-connected and standalone. They summarize the advantages and drawbacks of linear programming, intelligent techniques and fuzzy logic controllers, giving a clear overview of problems related to the control of intermitting RES and discussing the hybrid integration of CHP. In fact, electricity is just one aspect of the energy scenario, that inevitably needs to be linked to heat and cooling and their role in the decarbonization process, as reported by Werner et al. [17] and Rezaie and Rosen [18], where the authors also address the potential enhancements, especially in political and social awareness. Kang et al. [19] assess the implementation of photovoltaic thermal district heating concluding that cooling of PV cells and using PVT heat output to supply the source side of heat pumps to reduce their electric load are key ingredients for the success of the financial balance of the district. Behzadi et al. [20] provide an example of a possible PVT smart building to integrate in a district and perform an energy and exergy analysis of the system using TRNSYS to assess its functionality. Cogeneration and trigeneration on a university district level are assessed also in Rivarolo et al. [21], where a thermo-economic hierarchical methodology, sensitive to time variations, is used to analyze energy districts and intelligent poly-generation microgrids. Authors conclude that the trigeneration configuration optimized with this strategy is the best in terms of management, reduced size of thermal storages and reduced dependence on the national power grid. Mirzaei et al. [22] investigate the minimization of operation costs in an electricity, gas and district heating system. A 1.3 % reduction in operation costs is concluded by introducing multi-carrier energy storage in the integrated system. Also, the storage system has reduced the uncertainties of wind power generation by 20 % for the entire system.

Smart districts [23] and Microgrids (MGs) [24] with high penetration of RESs [25], have mostly both electrical and thermal energy sources and demands that use Distributed Energy Resources (DER) [26], Multi-Energy Systems (MES) [27] and Hybrid Energy Systems (HES) [28], which have been widely addressed by many researchers. Comodi et al. [29] discuss criticalities arising in central Italy when dealing with the revamping of district heating with a new cogeneration system based on gas turbines and thermal storage. They conclude that the current incentive scenario is not very attractive to implement more environmental-friendly solutions that involve TESS (Thermal Energy Storage System) “mainly because a convenient tariff structure for actuating load shifting does not exist”. Widmann et al. [30] studied district heating in combination with fluctuating solar and wind to derive an intelligent management system for the TESS that ensures the storage is at a low level in terms of its heat content just before an electricity demand is calling the CHP unit into operation. This, together with weather and energy forecasts from solar and wind allows for optimal operations of the CHP, with minimum numbers of switching on/off. Erdem et al. [31] performed an analysis to implement cogeneration and trigeneration in a conventional coal-powered scenario assessing the potential of total revamping of steam power plants.

Controlling the energy flow or implementing an Energy Management System (EMS) is of the most important parts of all MES/HES districts [32]. Salpakari et al. [33] applied a Rule-Based Controller (RBC) on a building and investigated its potential to maximize the self-consumption of PV panels. De Hoog et al. [34] demonstrated an application of a set of RBCs on batteries optimal scheduling and highlighted the fast response of these controllers in variations of conditions. In another study, Liu et al. [35] analysed two different energy management strategies using RBCs to achieve high energetic and economic performances in high residential buildings. Many researchers studied the application of Model Predictive Control (MPC) on MESs [36,37]. Kneiske et al. [38] studied the flexibility of a combined controller (MPC at high-level and Rule-Based Controller at low-level) under different operating modes to manage setpoints of a HES that can be self-sufficient up to 85 %.

Optimization of sizing [39,40], scheduling [41], operation [42], and energy management strategies [43] of the HESs are vital to reduce the carbon footprint. Awad et al. [44] studied the combination of PV, batteries, and μCHP (micro-Combined Heat and Power) and optimized the PV and battery sizes. In one study, Zhao et al. [45] used Genetic Algorithm (GA) to optimize the sizing of RES units having multiple objectives such as maximization of RES penetration, and minimization of costs and emissions. Considering gas and electricity tariffs, Schütz et al. [46] highlighted the effect of subsidies on the optimal size and operation of building energy systems. Zhang et al. [47] studied a HES in four different weather conditions and optimized the number of wind turbines, PV panels, and battery units using the Non-dominated Sorting Genetic Algorithm (NSGA-II) [48].

The implementation of many of the common strategies for decarbonization of the energy sector in the case addressed in this work is not straightforward, as it must comply with and account for the Italian

legislation on RES and their financial benefits, but also face the fact that a district in the centre of Rome is subjected to historical heritage conservation laws. These forbid significant changes in the architecture of historical buildings and structures, limit the installation of PV panels for visual reasons, and dig and install underground pipelines for methane, heat and electric and data cables.

Scope of the work

In this article, the clean energy transition of a district HES with multiple energy vectors in conjunction with energy production and storage systems is discussed, with the aim of deciding the energy efficiency intervention to be carried out and detailed in the public procurement procedure. A digital twin of the *ex-ante* scenario (the system as it is now) was developed in TRNSYS. Then all the possible interventions to increase the penetration of Renewable Energy Sources were considered, together with reduction strategies for CO_2 emissions, leading to the definition of an *ex-post* scenario that includes major renovations to the buildings and the improvement of their thermal insulation, lighting and conditioning systems. In this new digital twin, the energy flows are managed with a Python controller that governs the operation of all the components. The sizes or capacities of these energy conversion systems were optimized with the NSGA-II algorithm. The transition of the district was then evaluated with energy, financial and environmental performances for a preliminary study of the planned renovations, defining the interventions for the district renovations under the legal constraints of the national law on conservation of cultural heritage. This is a major issue in Italy, as these restrictions apply to most of the city centres, from large cities like Rome or Milan, to smaller municipalities with 10 k people, limiting the technical interventions available to install RES and renew the structures of the buildings.

The rest of this article is structured as follows: Section 2 explains the district details and two scenarios that were investigated. Section 3 provides all the modelling information, equations, and assumptions implemented in the simulation. In this section, the project scheme, control, and energy management strategy are explained. Section 4 highlights the energetic power balance, economic cost, and incentives. Moreover, the optimization algorithm, parameters, constraints, and objectives are discussed. Section 5 illustrates the results and follows with subsequent discussions.

2. Case study

The studied district is in the centre of Rome, Italy, and consists of several buildings for offices, short-term residencies and a small hospital. For this work, these buildings are grouped into three blocks here labelled as Block 0, Block 1, and Block 2 based on their proximity, Fig. 1. Each block is described through its electric and thermal loads, generations and storage.

Two scenarios are investigated to study the energy transition of the district. The district as it is, "*ex-ante*", fully dependent on the national electricity grid to cover its load and on the national gas grid to fuel gas-fired boilers that satisfy the heat demand. The cooling demand is covered by electric air conditioning systems. The second scenario is called "*ex-post*" by which the district energy metabolism was reimagined aiming at reducing its environmental impact, while still complying with the strict heritage preservation laws that apply to the centre of Rome. In this case, the major limitation comes from the impossibility of drilling below the buildings to install new pipelines for heat exchange between different blocks, the impossibility of installing wind turbines and limitations on the installations of PV panels due to visual impact. Thus, in the ex-post scenario, a set of PV panels and battery banks are introduced to all district blocks. Each block also entails a micro-turbine cogeneration set coupled with an absorption chiller, mainly to cover heat and air-cooling and then assist in electricity generation. Due to the mentioned restrictions, each block can exchange electricity with the others through the existing power grid, while thermal energy can only be exchanged between the buildings inside each block. The overall goal is to cut the energy costs and CO_2 emissions of the whole district.

The electric loads are measured at each building's POD (Point Of Delivery) using 2nd generation smart meters in quarter hour form and further aggregated to shape each block's consumption profile. Loads reported here were collected in 2019 and provided by the Distribution Service Operator (DSO). Heating loads are calculated from the gas consumption and the domestic hot water demand of each building's operating boiler in the "ex-ante" scenario. Cooling loads are constructed based on the activities of the air conditioners and their electricity consumption profiles.

Hourly loads of the "ex-post" scenario for each block are shown in Fig. 2 for electric (left) and thermal (right) demand. Yearly energy demand is shown in Table 1 and in general highlights how Block 0 has the

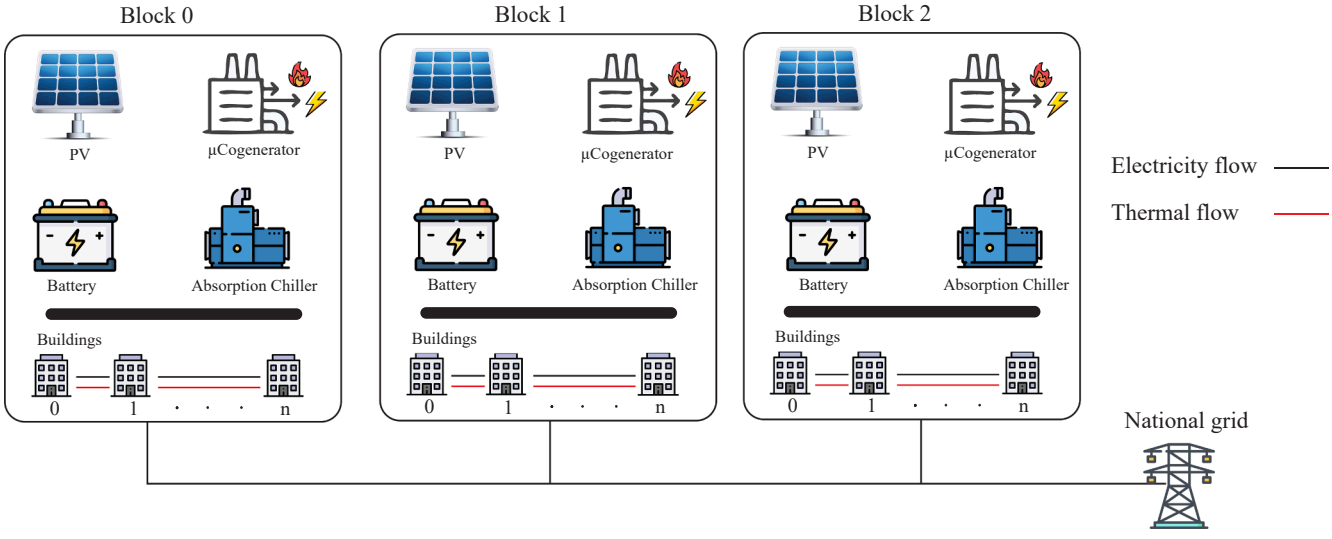

Fig. 1. District schematic with the sub-grouped block details.

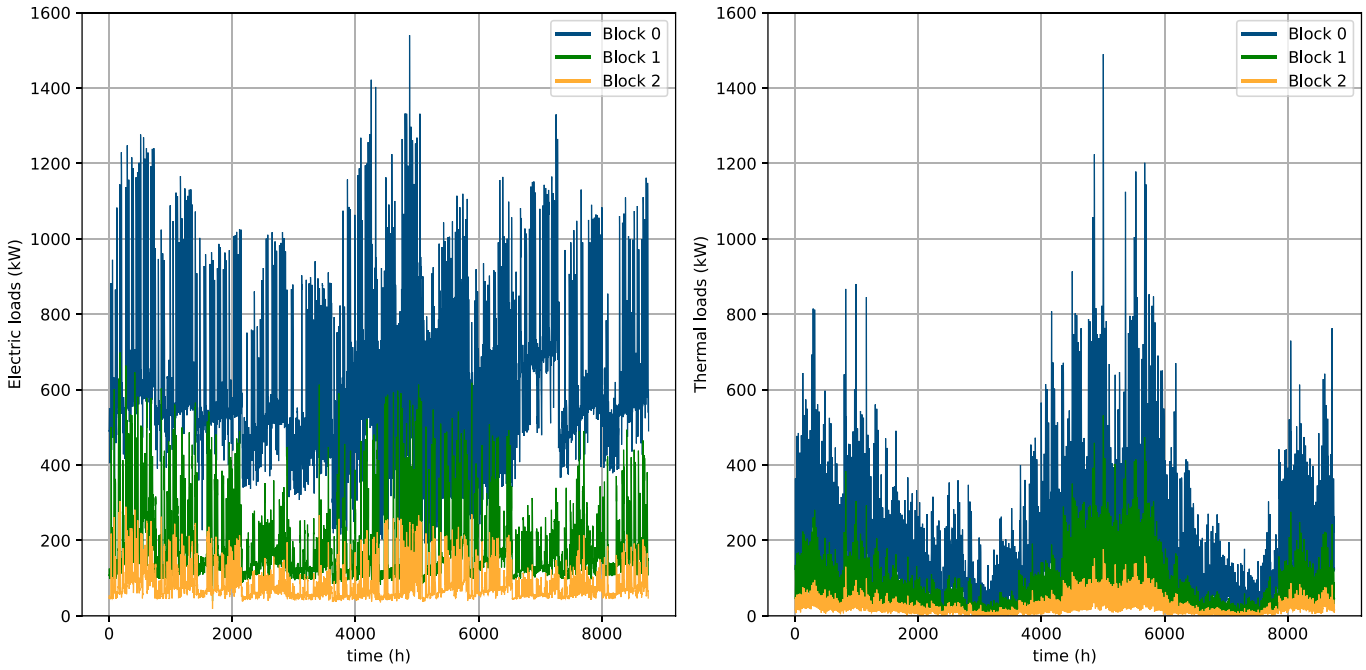

Fig. 2. Electric loads (left) and thermal loads (right) of the district blocks in the ex-post scenario.

Table 1
Electric and thermal loads of all blocks in both scenarios.

	Electric (MWh)		Thermal (MWh)	
Block	ex-ante	ex-post	ex-ante	ex-post
0	6538	5628	824	1734
1	2042	1704	279	617
2	855	744	98	209

highest demand, followed by Block 1.

3. Modelling of energy and financial flows

The project model scheme is shown in Fig. 3 with all the components and their interconnections. The input data consists of the loads which are communicated with the controller and the weather data used by PV panels. At every time step of the simulation, all energy conversion units

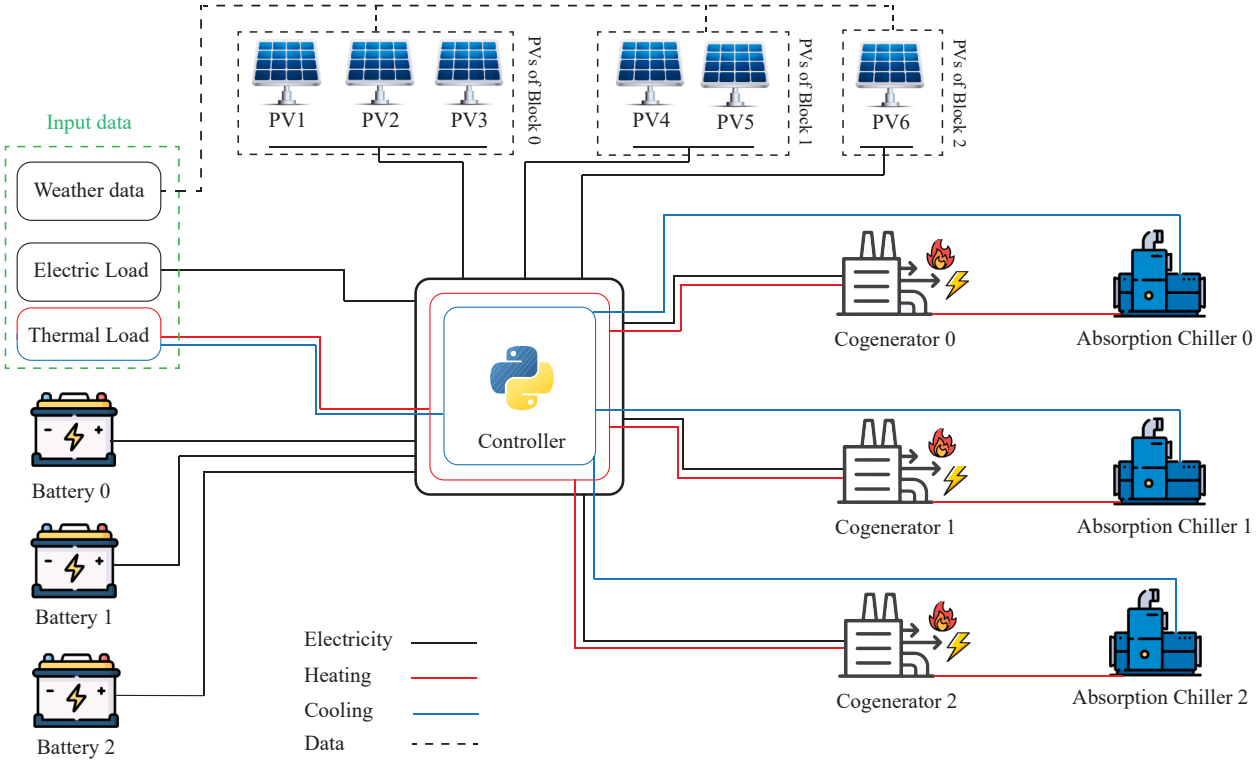

Fig. 3. TRNSYS scheme for ex-post scenario.

(PV panels, cogenerators and chillers) as well as the battery storage systems report their operation condition to the controller. Based on the magnitude of the loads and the current operating condition of the system, the controller implements a defined logic and dispatches new operation commands to each unit. Details of the controller logic and all the modelled energy units are discussed in the following sections.

The district energy metabolism is numerically simulated using TRNSYS 18.0 [49]. The software has been extensively validated in [49] and [50]. However, exclusive research is conducted on similar energy system units implemented in this current work [51–54]. For example, Axaopoulos et al. [55] reported on 99.7 % accuracy of the TRNSYS photovoltaic model compared to the experimental data. Kanyarusoke et al. [51] experimentally validated TRNSYS Type 94 (changed to Type 103 in TRNSYS 18.0) using a fixed slope PV panel. The model is validated by both short-term (one month) and long-term (one year) evaluations where the modeling results were in good agreement with the experimental data. Therefore, these validated energy units are befitting tools to rely on and implement in further energy system designs.

3.1. Meteorological data

The weather data are provided via Type 15-6 in TRNSYS, according to Meteonorm V5 [56] published by Meteotest [57]. This district studied here is in Rome, Italy (41.9028° N, 12.4964° E). The annual maximum temperature is 34.25 °C and maximum solar irradiance is 860.85 W/m^2.

3.2. PVs

PV panels are simulated in TRNSYS using Type 103 [49] representing polycrystalline PV panels. The model follows a four-parameter equivalent circuit mode and is equipped with an MPPT (Maximum Power Point Tracker). The technical details and governing equations of PV panels are reported in Appendix D. PV panels are mostly installed on the rooftops and partly on the façade of one building. Table 2 summarizes the capacities, array slopes, and annual production of PV panels.

3.3. Batteries

Lead-acid batteries are selected for the district due to their low costs, large capacities, and stationary applications; they are simulated with TRNSYS Type 47 [49] that takes power as input and through energy balance defines the battery's State of Charge (SoC). The battery operates in conjunction with the controller to manage its charge and discharge conditions. The technical details and governing equations are reported in Appendix D.

3.4. Cogenerators

The cogeneration units are modelled using Type 120 [49] calculates the fuel consumption based on the generated electricity. Fuel efficiency curves could be inserted into this model to resemble the desired characteristics of a cogeneration unit. Absorption chillers use the recovered heat of the cogeneration units and provide a stream of chilled water via an absorption cycle. Type 676 [49] represents a steam-fired absorption chiller in TRNSYS that takes steam as an energy source and uses the manufacturer's performance data to calculate the output chilled energy. The technical details and governing equations are reported in Appendix D.

3.5. Energy management strategy

The energy management strategy is based on a real-time Rule-Based Controller (RBC), implemented in an in-house Python code that manages the energy flows in the district. The Python controller is linked directly to the TRNSYS project through Type 3157 [58] as shown in Fig. 3. The controller has multiple responsibilities and is designed to make decisions based on upcoming conditions. The advantages of the RBC over other control methods, such as simplicity and fast response to the change of conditions, were the main reasons for selecting such a controller.

The control logic of the district can be summarized in the following points:

- All three blocks can share the electricity generated by the PVs and cogeneration units through the national power grid. Excess is sold to the supplier, which also provides the energy in case of insufficient internal production.
- The electricity surplus of each block is used first to fulfil the energy of the rest of the district with a priority logic from block 0 to block 1 and then block 2.
- Batteries are recharged if the district energy demand is completely fulfilled. In this case each block recharges first its own battery and then the others according to the aforementioned priority. While batteries can get charged with excess electricity from other blocks, each battery can get discharged only to its own block. The SoC of batteries is controlled to vary between 20 % and 85 % to avoid battery overcharging and drainage.

Table 2
Blocks, building, and PV panel details.

Block ID	Building ID	PV tilt (°)	PV nominal power (kW)	Annual production (MWh)
0	1	90	474.2	714.2
	2	36	99.4	142.0
	3	36	178.8	284.0
1	4	36	96.0	78.6
	5	36	716.4	1146.0
2	6	36	357.3	575.0

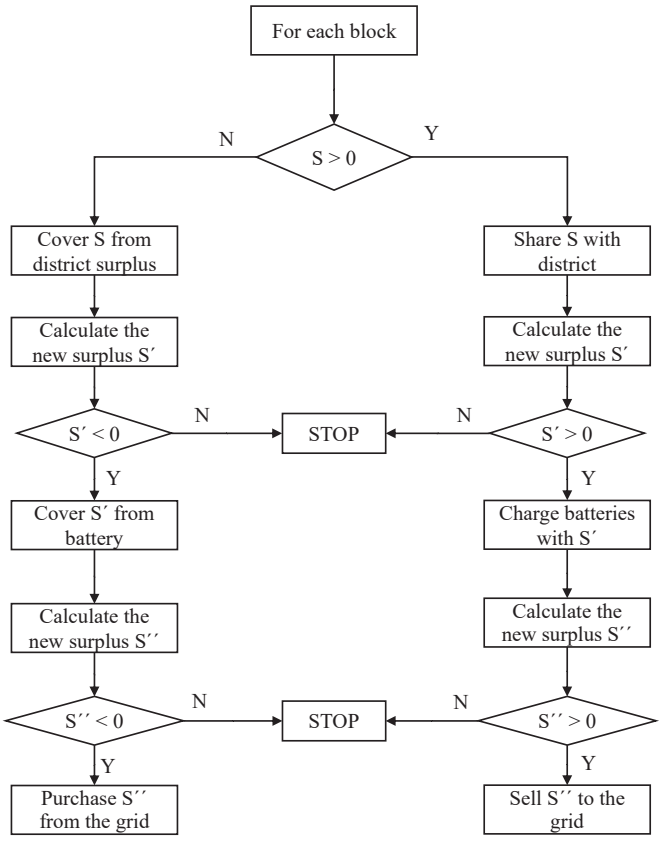

Fig. 4. Simplified energy management system flowchart.

- Cogeneration units are activated only when the thermal load is at least equal to 80 % of the nominal thermal power of cogenerators. The controller also prevents cogenerators from switching ON and OFF frequently. If the system is ON and the thermal load falls below 80 % of the nominal thermal power, the controller switches the system OFF only if there has been no energy request in the last 24 h.
- Absorption chillers' control logic follows the operation of the cogeneration units accordingly. Also, they switch OFF if the thermal load is less than 3 kW to avoid damages due to frequent ON/OFF switching.

Fig. 4 shows a summary of the general operating flow chart of the controller. The detailed controller flowchart is depicted in Appendix C.

4. Optimization

An optimization problem is defined to find the optimal size or capacities of the developed energy system units. The target parameters of the optimization are the size of PV panels, the capacity of batteries, and the size of cogeneration units. There are 12 parameters in all three blocks as reported in Table 3. These parameters are constrained by several bounds. The imposed constraints for PV panels correspond to the limited surface area of the buildings, for batteries are their market availability and for the cogenerators are the load coverage sufficiency.

Optimization is driven by the NSGA-II algorithm implemented in a Python module that uses the Pymoo library [59]. The algorithm randomly generates a first set of populations where each candidate represents a different energy system configuration. Then the algorithm calls TRNSYS to evaluate the performance of each individual candidate via the objective functions and initiates the next generation accordingly. This process continues until the algorithm finds the optimal solutions.

4.1. Objective functions

The target of this multi-objective optimization is to run the district with the most satisfying energetic and economic performance. Therefore, two different metrics are considered as objective functions. The first objective function, to be maximized, is self-consumption:

$$OF_1 = self\ consumption = P_{pv} + P_{cog} + P_{batt} + P_{ex} - P_{load} = P_{grid} \quad (1)$$

Table 3
Optimization parameters, constraint bounds and variation step sizes.

Parameter index	Parameter description	Block index	Lower bound	Upper bound	Step
1	PV panels of building 1	0	0	472.5 kW	
2	PV panels of building 2	0	0	100.8 kW	
3	PV panels of building 3	0	0	179.6 kW	1.575 kW
4	PV panels of building 4	1	0	97.7 kW	(5 panels)
5	PV panels of building 5	1	0	715.1 kW	
6	PV panels of building 6	2	0	356 kW	
7	Capacity of battery 0	0	0	500 kWh	
8	Capacity of battery 1	1	0	500 kWh	20 kWh
9	Capacity of battery 2	2	0	500 kWh	
10	Size of cogeneration 0	0	0	500 kWe	
11	Size of cogeneration 1	1	0	300 kWe	5 kWe
12	Size of cogeneration 2	2	0	200 kWe	

in which P_{pv}, P_{cog}, P_{batt}, P_{ex}, and P_{load} are respectively the power of PV panels, cogenerators, batteries, exchanged amount of energy between blocks, and the load. P_{cog} and P_{load} account for both electric and thermal energy.

The second objective function, to be minimized, is the economic cost of the components. To this end, The Net Present Value (NPV) of the cost and benefit sources are considered. Capital expenditure (*CAPEX*) and operational expenditure (*OPEX*) of the system components as well as consumed fuel cost, grid interaction costs/benefits, and received incentives are listed in Eq. (2).

$$OF_2 = NPV = \sum_{i=1}^{n} CAPEX_i + \sum_{t=1}^{10} \frac{V}{(1+r)^t} \quad (2)$$

where r is the discount rate (assumed to be 4 %) and the time horizon t of this analysis is assumed to be 10 years based on the usual life span of lead-acid batteries. V is the variable costs/benefits and is formulated as:

$$V = \sum_{i=1}^{Ncogen} OPEX_i - Incentive_i + \sum_{j=1}^{Npv} OPEX_j + \sum_{k=1}^{Nbatt} OPEX_k - \sum_{l=1}^{Nblock} Grid_{cb,l} \quad (3)$$

in which N_{cogen}, N_{pv}, N_{batt}, and N_{block} are the number of cogeneration units, PV panels, batteries, and blocks respectively. $Grid_{cb}$ is the district cost/benefit due to grid interaction. In addition to the mentioned objective functions, other metrics are introduced to evaluate the proposed system performance. The Levelized Cost Of Energy (*LCOE*) is a metric to analyze the technical and economic potential of an energy system during its lifetime. It is calculated as the ratio of the total discounted life cycle costs to the discounted generated energy:

$$LCOE = \frac{OF_2}{\sum_{t=1}^{ny} \frac{E_{gen,tot}}{(1+r)^t}} \quad (4)$$

Table 4
Capital and operation costs of system components.

Component	CAPEX	OPEX ($/kW)	Source
PV	1400 ($/kW)	16 ($/kW-year)	[60]
Battery	549 ($/kWh)	10 ($/kW-year) + 0.03 (c$/kWh-year)	[61]
Cogenerator	2120 ($/kWe)	1.3 (c$/kWh)	[62]
Absorption chiller	1800 ($/ton)	0.1 (c$/ton-h)	[62]

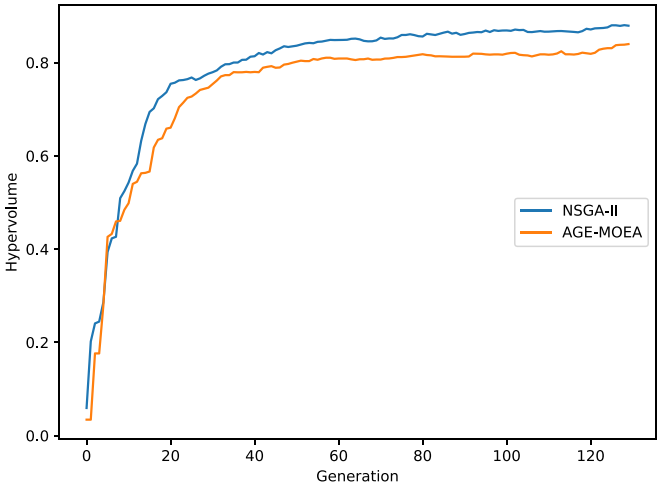

Fig. 5. Performance comparison of NSGA-II and AGE-MOEA algorithms by hypervolume metric.

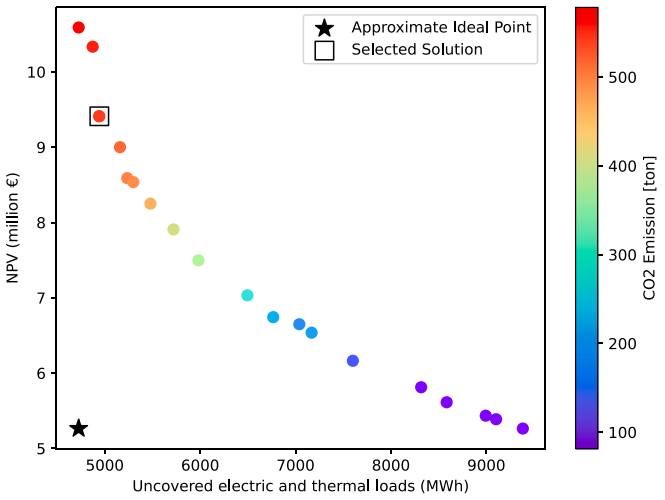

Fig. 6. The Pareto-front of the optimization of devices in the district.

in which $E_{gen,tot}$ is the total generated electrical and thermal energy and ny represents the system operation lifetime. Another indicator is the payback (PB) period which is the number of years required to recover the cost of an initial investment and is calculated using the ratio of total initial costs to the annual cash flow of saved costs:

$$PB = \frac{\sum_{i=1}^{n} CAPEX_i}{Annual\ saved\ cost} \tag{5}$$

where n is the number of purchased units. The $LCOE$ and PB are further used in the result section to analyse the economic feasibility of the energy system.

4.2. Economic costs and benefits

CAPEX and OPEX of the components are listed in Table 4.

Natural gas cost due to the operation of cogeneration units has different values in every year based on the prices reported by ARERA (Italian for Regulatory Authority for Energy Networks and the Environment) [63]. The reported price span is between 2014 and 2021, however, the average values of this time span are used in the current research to smooth the price oscillations for non-domestic users. Table A.1 in the appendix illustrates these values in detail.

4.2.1. Grid interaction costs/benefits

The monthly purchasing electricity price for a non-domestic user is adapted from ARERA [64]. They have been monthly averaged from 2017 to 2020 to avoid occasional fluctuations.

The eventual surplus of generated electric power is sold to the grid following the regulations of GSE (Italian for Energy Services Manager) [65]. The detailed purchasing and selling prices are tabulated in Table A.2.

Finally, having the grid interaction power (P_{grid}) from the power balance of Eq. (1) and the unit electricity cost/benefit price from Table A.2, the total grid cost/benefit can be calculated as:

$$Grid_{cb} = P_{grid} * C_g \tag{6}$$

where C_g is the unit purchasing/selling price of electricity.

4.2.2. Incentives on high-efficiency cogenerations

A mechanism came into force in 2005 to promote energy efficiency in Italy. This mechanism entitles the cogeneration units to receive energy efficiency certificates also known as *White Certificates*. Each certificate equivalently saves one ton of oil. The number of certificates is proportional to the Primary Energy Saving (PES) index. Detailed calculation of the incentive structure is reported in Appendix B.

4.3. Optimization algorithm performance

In addition to the NSGA-II, the problem is solved using a second algorithm called as Adaptive Evolutionary Algorithm for Many-objective

Table 5
Size of PV panels, batteries, and cogeneration units of the selected solution.

PV capacity (kW)						Battery capacity (kWh)			Cogenerator size (kW)		
PV1	PV2	PV3	PV4	PV5	PV6	Batt0	Batt1	Batt2	Cog0	Cog1	Cog2
446	88	176	49	712	345	300	20	20	105	55	10

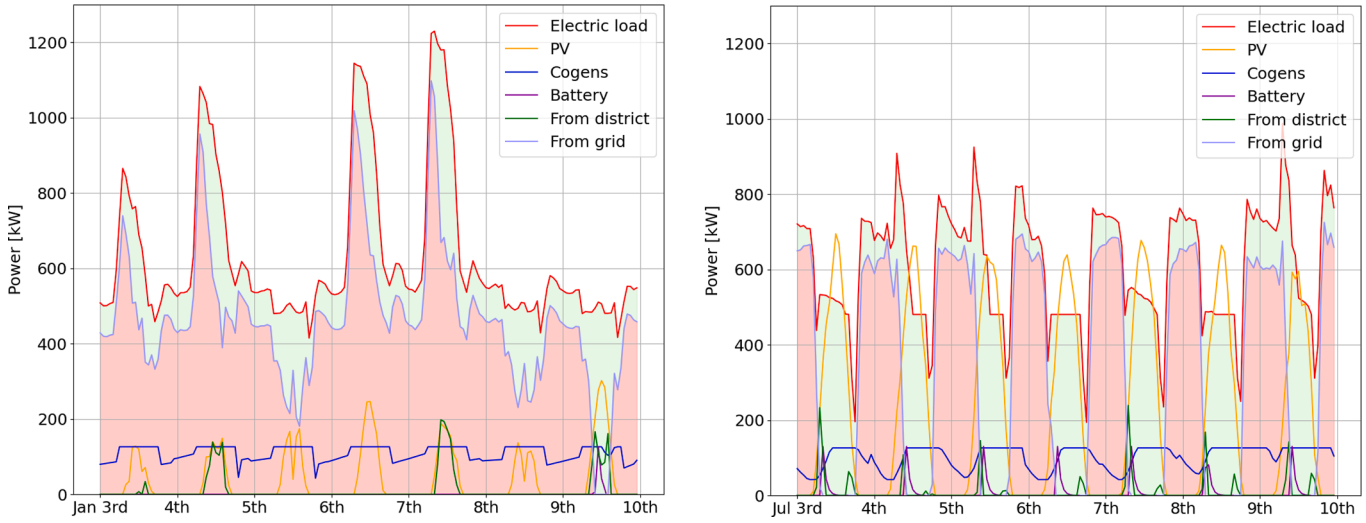

Fig. 7. Electric metabolism of Block 0 during a week in January (left) and July (right). In green and red respectively the amount of electricity produced in the district and bought from the grid.

Optimization (AGE-MOEA) [66]. The performance of these algorithms is compared with each other using Hypervolume metric [67] in which target solutions are not required and a reference point is used instead. It calculates the area or volume dominated by the solution set and the reference point in each generation.

The convergence criterion is met after 130 generations and the hypervolume metric of both algorithms is plotted in Fig. 5. In this case, the NSGA-II outperforms the AGE-MOEA as it shows a higher speed to reach higher domination rates with respect to the same reference point for both algorithms. Therefore, the NSGA-II is selected as the main algorithm for the described optimization problem.

4.4. Optimization results

In Fig. 6, the Pareto front of the optimization is plotted. For the selected solution, the algorithm choses the highest possible size of PV panels (since there is an instantaneous electricity sharing between blocks and the surplus). Regarding batteries, Block 0 has a larger battery compared to other blocks due to its higher electric load. The algorithm selects relatively low cogeneration capacities for Blocks 1 and 2 since there is no thermal energy sharing between district blocks to avoid

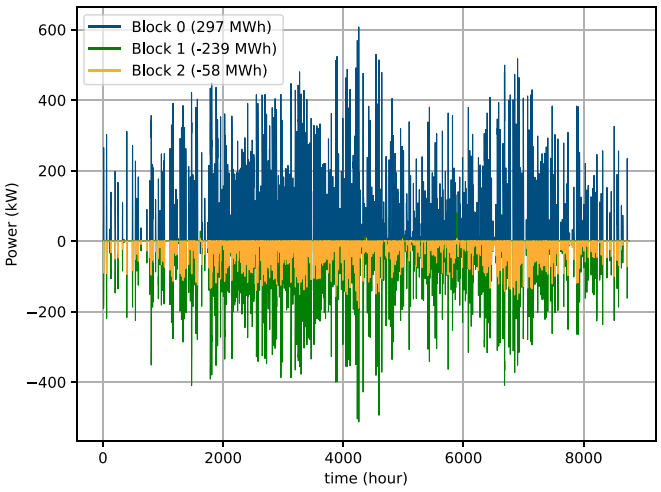

Fig. 10. Exchanged electricity of each block to (−) / from (+) the district.

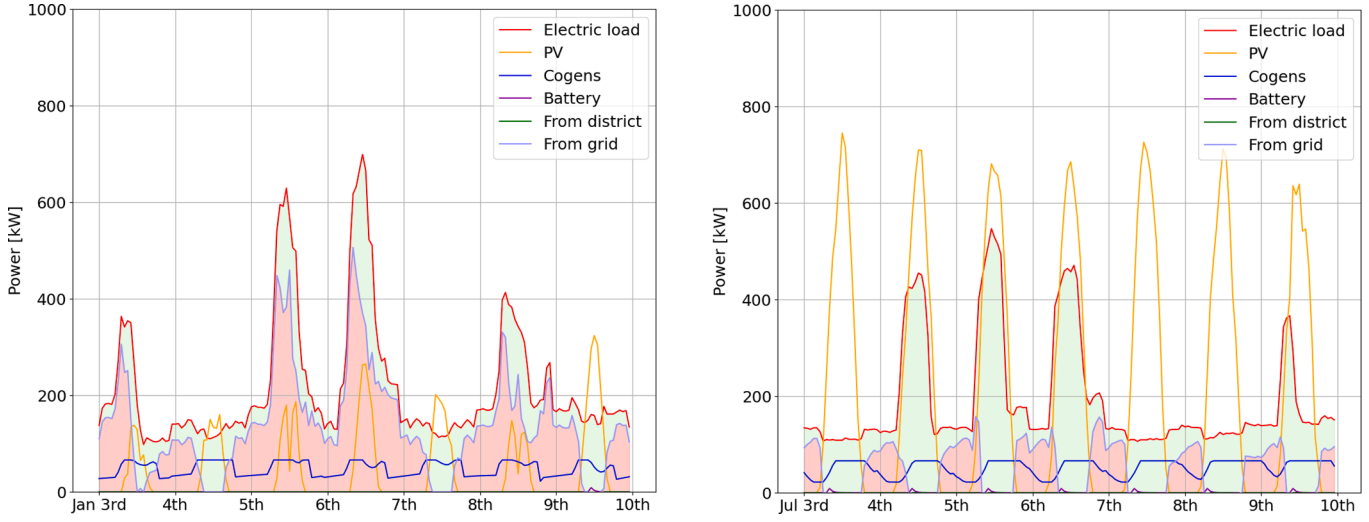

Fig. 8. Electric metabolism of Block 1 during a week in January (left) and July (right). In green and red respectively the amount of electricity produced in the district and bought from the grid.

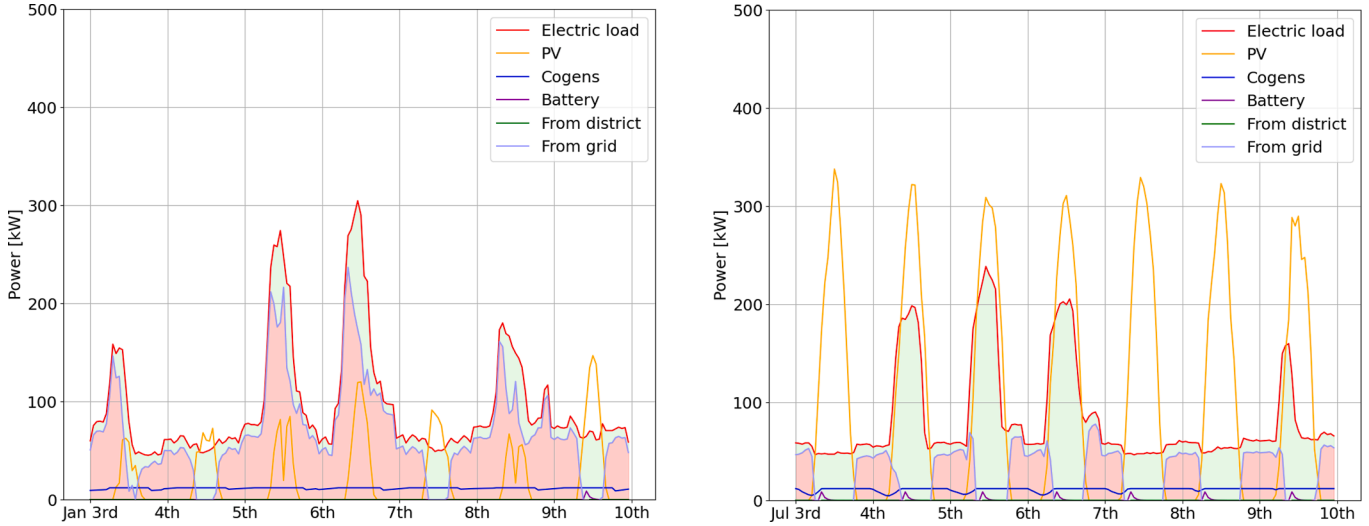

Fig. 9. Electric metabolism of Block 2 during a week in January (left) and July (right). In green and red respectively the amount of electricity produced in the district and bought from the grid.

dumps of production excess.

The genes of the selected solution are reported in Table 5 and the entire Pareto front is tabulated in Table A.3. A decomposition function [68] is used to select the solution based on the importance of the optimization objective functions. Inserting an 85 % and 15 % weight on energetic and economic performances leads to selecting a specific point among all solutions (shown with a square in Fig. 6). These weights are deliberately chosen for ease and better visibility of further plotting and discussion of results.

5. Results

This section summarizes the energy metabolism of the ex-post district weekly, monthly, and annually and then compares it with the ex-ante scenario.

The electrical energy analysis of the three blocks is shown respectively in Figs. 7 to 9 for a week in January and another in July. First, the number of PVs is not sufficient to cover the energy demand of Block 0, and cogens can only provide a fraction of the required load, as dimensioned to cover the thermal load. However, the availability of space on the rooftops of Blocks 1 and 2 is sufficient to cover the daytime in the summer and during most of the middle seasons (not shown here). This scenario is sufficient to have an impact on the CO_2 emissions of the district as will be discussed in the following. Finally, from these figures is also evident that Block 0 is the one that receives most of the district surplus, as only a fraction of the overall surplus is absorbed by the other two blocks. A scenario like this can be sustained only because the whole district entails just public administration buildings.

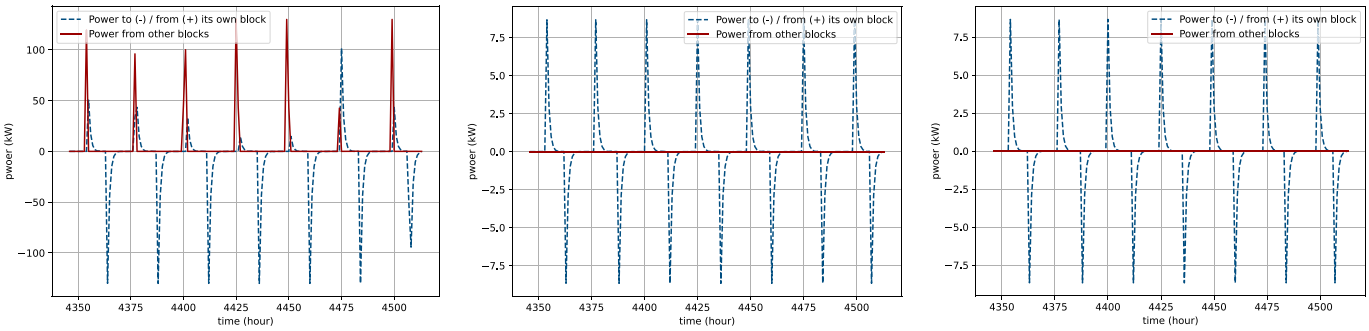

Fig. 11. Interaction of Block 0 (left), 1 (center) and 2 (right) batteries in the first week of July.

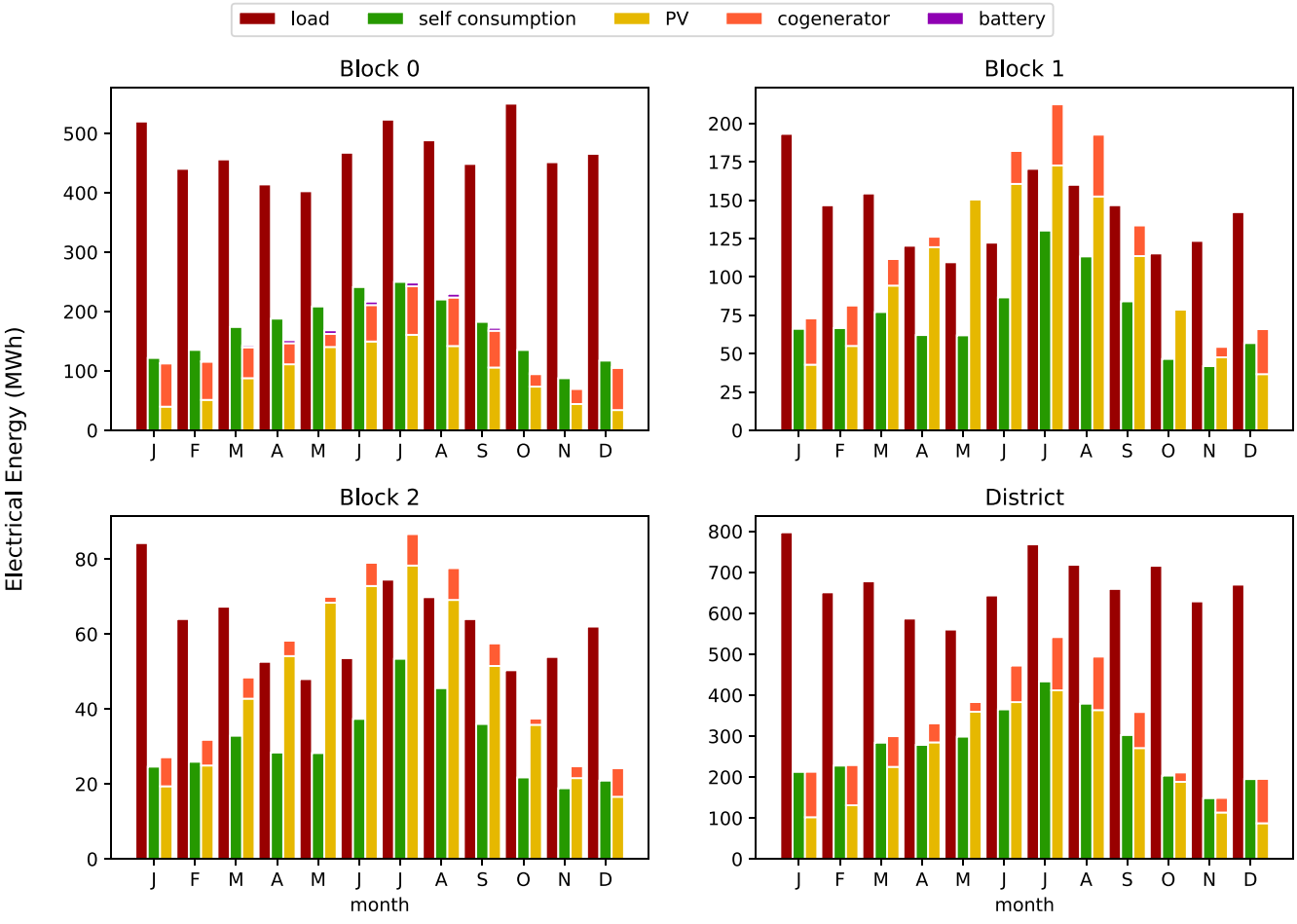

Fig. 12. Monthly electricity performance of all blocks and the entire district.

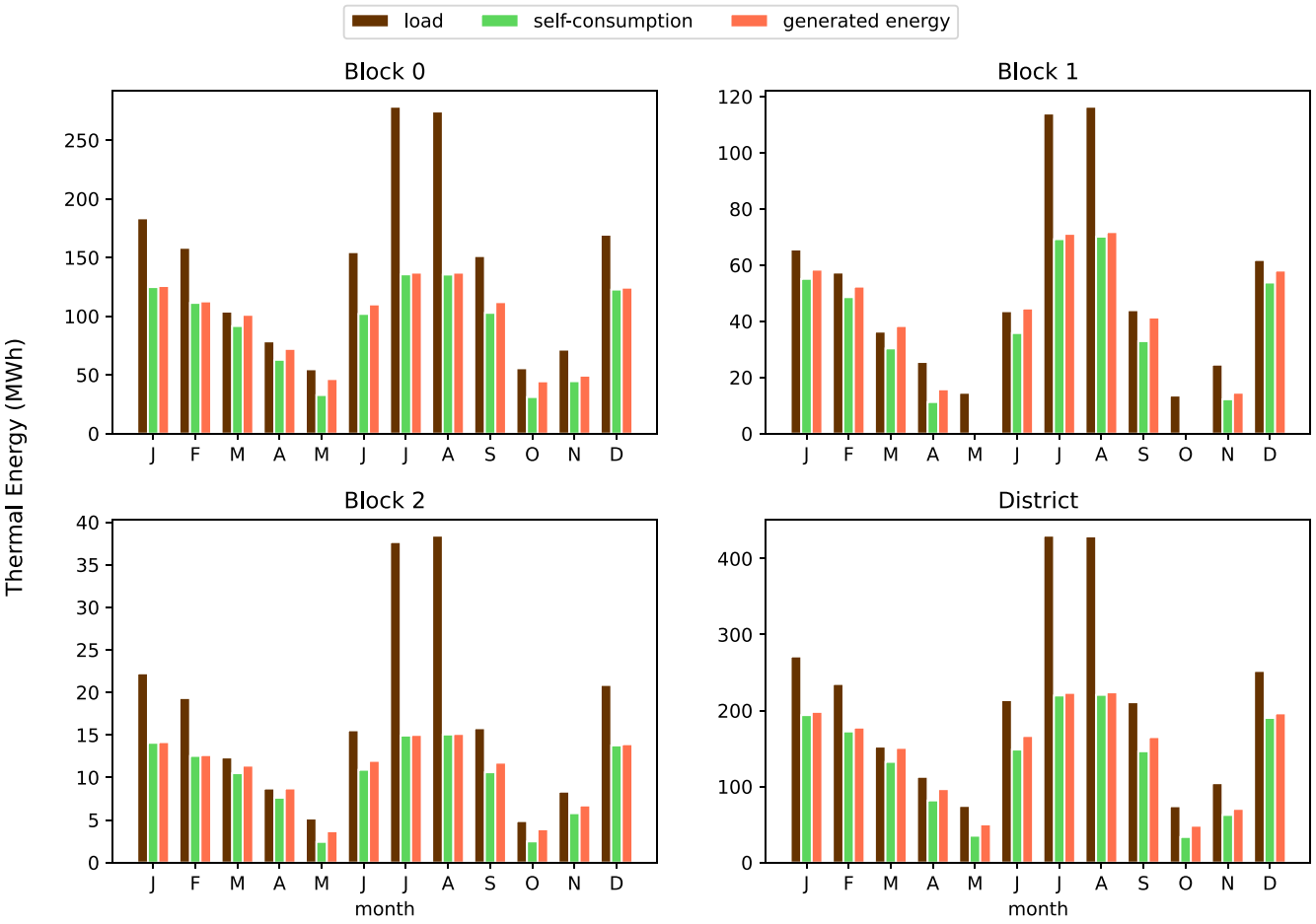

Fig. 13. Monthly thermal performance of all blocks and the entire district.

One of the advantages of the district is that each block has instantaneous interaction with others to share electricity. Fig. 10 shows the amount of energy each block receives from (+) or delivers to (−) the district. For example, Block 1 has relatively high PV capacity and low electric load so it can provide its surplus to the other blocks of the districts; on the contrary, Block 0 receives energy from the rest of the district almost all the year.

Each block is equipped with a battery bank to store energy in case of surplus and assist in satisfying the load. As discussed in Section 3.5, the controller manages the battery SoC. Each battery is allowed to get discharged only to its associated block and is allowed to get charged from the RES overproduction of all blocks. The behaviour of the associated batteries on each block during the 1st week of July is shown in Fig. 11. Blocks 1 and 2 use the excess of PVs to recharge their own batteries and then the excess is delivered to the battery in Block 0.

The energy analysis of the district is also reported monthly. The

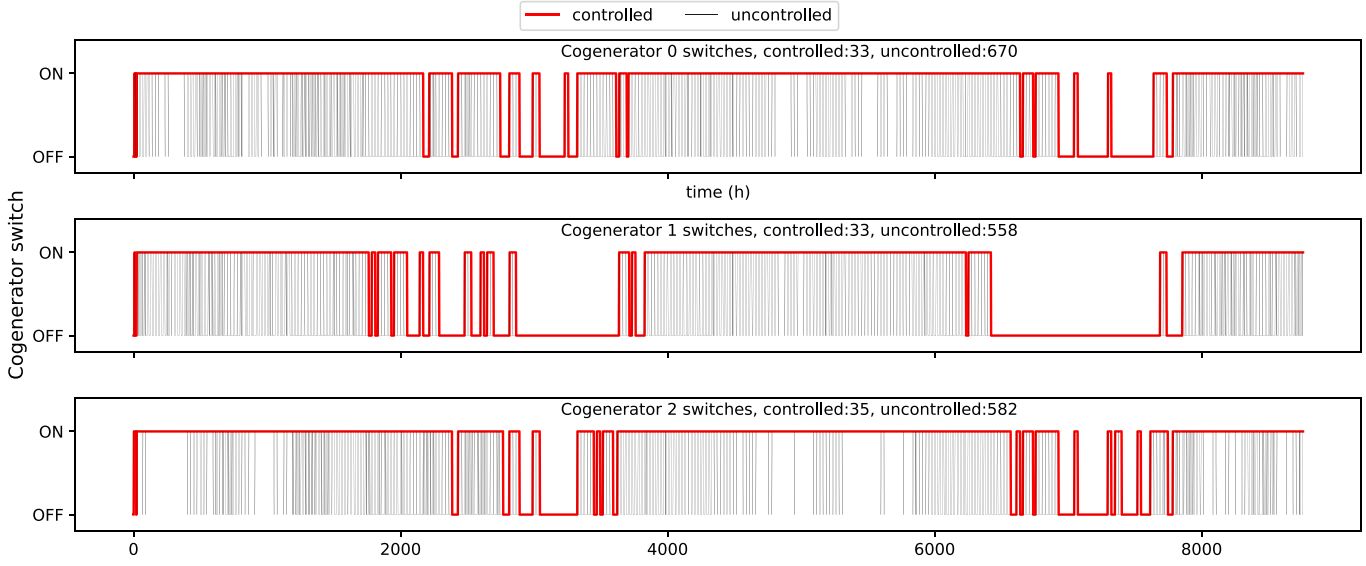

Fig. 14. Controller performance on ON/OFF switches of all cogeneration units.

contribution of energy sources and energy storage is shown in Fig. 12 for each block separately and for the entire district. Block 0 load cannot be covered in any month of the year from renewable sources. Block 1 and Block 2 have higher PV productions than their electric loads between April and September. They assist Block 0 during these months to achieve higher amounts of self-consumption in the district. The role of batteries is more effective in warm months of the year as the PV production is higher. Batteries contribution is relatively low due to their low capacities w.r.t the load and in fact, the main reason to install them is to provide backup in case of emergency to specific loads in the district. They can cover the demands of the system in very specific hours, but they are not beneficial from the entire district's point of view.

The thermal behaviour of the district and all blocks is shown in Fig. 13. The capacity of cogeneration units of Block 0, Block 1, and Block 2 are 105, 55, and 10 kWe respectively. Regarding the entire district, a considerable portion of the thermal load is covered in the cold months of the year. In summer, the load coverage has a lower percentage since the load is much higher having the same capacity of cogenerators. In fact, the optimal sizing accomplished by NSGA-II, suggests that the cogeneration units must be undersized to satisfy the economic costs as well. Moreover, the energy from the cogenerators is quite close to the self-consumption, which means the controller has managed the operation of cogeneration units to have the least possible amount of dumped energy, although there were some boundaries on the operation strategy of these units.

As already mentioned in Section 3.5, one of the main objectives of the controller is to monitor and adjust the operations of the cogeneration units. Fig. 14 shows that the controller was able to reduce and limit the ON/OFF switches of cogenerators for example from 670 times to 33 times for Block 0. This will avoid the degradation of cogeneration units and increase their lifespan.

The annual electric summary of the district and each individual block is shown in Table 6. The dependency of the entire district on the national grid reduced from 8076 MWh (ex-ante) to 4150 MWh (ex-post). All blocks are receiving more benefits from their associated PV panels rather than the other internal energy sources. This trend is even intensified in Blocks 1 and 2. The share of batteries with their current capacities is quite low. Therefore, we could either increase their capacities and bear more economic costs or remove them from the district totally.

Table. 7 summarizes the annual thermal performance of the district. The thermal demands of each block and the whole district are satisfied approximately by 60 %. It is worthwhile noting that the amount of dumped heat w.r.t generated heat is relatively low, which implies the optimum sizing of the system and desirable performance of the controller. If the district was in another location without the current strict urban limitations of Rome, there would be a thermal exchange between the blocks leading to higher thermal performance.

The overall performance of the district is compared in Table. 8. Results of the old scenario ex-ante) and the district scenario (ex-post) are reported. Dependency on the national grid is reduced by 68.2 %. The amount of primary energy consumption and CO_2 emissions are calculated based on the guidelines of "Requalification of the Buildings of the Central Public Administration" [69] and are reduced by 55.73 % and 56.02 % respectively.

Table 9 demonstrates the economic comparison of the two investigated scenarios. It includes the CAPEX, OPEX and generation cost of energy. In the ex-ante scenario, the generation cost includes the grid electricity import and the burnt fuel of the boilers, however, in the ex-post scenario, it contains the received incentives due to the implementation of high-efficiency cogenerators as well. Unfortunately, CAPEX and OPEX data of the ex-ante scenario is not available, however, the 48.9 % decrease in generation cost justifies the economic advantage of the ex-post scenario.

The LCOE of the proposed energy system is calculated by Eq. (4) and is equal to 196 €/*MWh*. A sensitivity analysis is conducted for the LCOE to assess the effects of involved system key parameters, including

Table 7
Annual thermal summary of all blocks and the district.

Block	Load (MWh)	Delivered heat (MWh)	Covered load (MWh)	Covered load (%)	Deficit heat (MWh)	Dumped heat (MWh)
0	1734	1172	1098	63	646	30
1	617	466	419	68	198	28
2	209	129	121	58	89	3
District	2560	1767	1638	64	933	61

Table 8
Energetic and environmental comparison of ex-ante and ex-post scenarios.

Scenario	Purchased energy from grid (GWh)	Primary energy consumption (GWh)	CO_2 emission (ton)
ex-ante	13.05	32.05	6196
ex-post	4.15	14.19	2725
delta (%)	−68.20	−55.73	−56.02

Table 9
Economic comparison of ex-ante and ex-post scenario.

Scenario	CAPEX (k€)	OPEX (k€)	Generation cost (k€)	Incentives (k€)
ex-ante	–	–	687	0
ex-post	5473	485	351	35

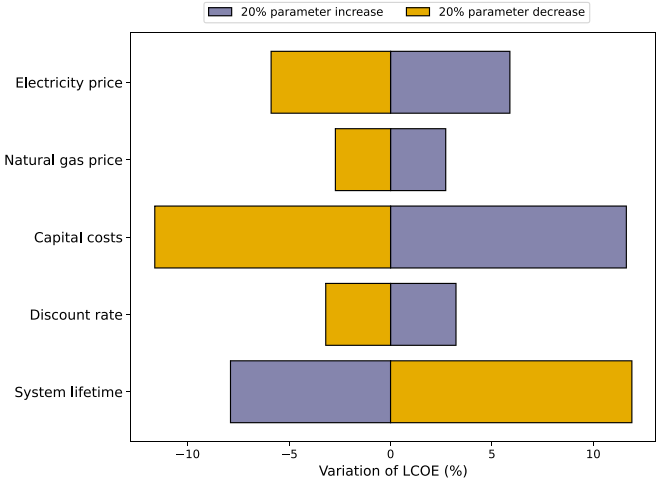

Fig. 15. Sensitivity analysis for levelized cost of energy with 20% variation of five key parameters.

Table 6
Annual electric summary of all blocks and the district.

Block	Load (MWh)	PV (MWh)	Cogenerator (MWh)	Battery (MWh)	Exchanged energy to(−)/from(+) district (MWh)	Covered load (MWh)	Energy to(−)/from(+) grid (MWh)
0	5628	1140	651	43	297	2053	3497
1	1704	1225	239	3	−239	893	477
2	744	555	68	3	−58	374	176
District	8076	2920	958	49	0	3320	4150

electricity and natural gas prices, capital costs, discount rate and the system lifetime. The analysis proceeds based on the variation of one parameter at a time and the other factors are assumed to be constant. Fig. 15 depicts that the LCOE is most sensitive to the capital cost variations by ± 8.7 % since it counts as the most significant economic drive of the system. The LCOE is found to be less sensitive to the natural gas price and the discount rate compared to the electricity price because the electric demands shape the larger portion of the total district loads. System lifetime has an inverse but favourable effect on the LCOE, meaning that a higher system lifetime leads exponentially to lower LCOEs. One can conclude such improvement requires a higher quality on the maintenance of the energy units as well as a proper controller to avoid unit degradation using an advanced energy management system.

The payback period evaluates the economic feasibility of the energy system. It is calculated according to Eq. (5) and is reported to be 20 years for the proposed energy system. The value is more than twice what should be considered acceptable, however, entails high-capex building renovations that were considered in the calculations and that would have been carried out even without the overhaul of the energy consumption.

6. Conclusions

This research presents a study on the energy transition of a district in Rome toward a sustainable energy scenario. The district is close to the city center and thus partially falls under historical heritage conservation laws that do not allow major overhaul of structures and forbid digging of new pipelines for heat exchange, leaving a limited number of possible technical solutions. Here two scenarios were analyzed: one *ex-ante* with the district current electrical, heating and cooling systems. And an *ex-post* scenario where, exploiting the physical adjacency of different blocks and significant availability of rooftop surfaces from buildings belonging to the same public administration, it was possible to design a system able to include solar panels and BESS and to implement a trigeneration scenario that provided significant reduction of primary energy consumption and CO_2 emissions. The energy, financial and environmental impact in terms of CO_2 emission metabolism of the district were simulated in TRNSYS, implementing an in-house Energy Management System (EMS) designed in Python to control the energy flows. The ex-post scenario that entails an integrated management of electric and thermal loads was optimized using an NSGA-II algorithm to size the components of the district. The introduction of PV panels, batteries, and high-efficiency cogenerators and absorption chillers managed by a smart controller allowed reducing the primary energy consumption and CO_2 emissions respectively by 55 % and 56 %, reducing the amount of purchased energy from the grid and generation cost by 68.2 % and 48.9 %. The levelized cost of energy is equal to 196 €/MWh and a sensitivity analysis indicates its highest sensitivity on the capital costs. The payback period is estimated as 20 years but entails capital costs relative to a major renovation of the buildings that were already in the planning.

Declaration of competing interest

The authors declare that they have no known competing financial interests or personal relationships that could have appeared to influence the work reported in this paper.

Data availability

The authors do not have permission to share data.

Acknowledgments

This research is supported by the Ministry of University and Research (MUR) as part of the European Union program NextGenerationEU, PNRR - M4C2 - ECS_00000024 “Rome Technopole” in Flagship Project 1 “Clean energy transition and circular economy: materials, bioenergy, green chemistry, green hydrogen and alternative fuels, renewable energy communities, isolated energy systems and smaller islands“ and by Regione Lazio under agreement with Department of Mechanical and Aerospace Engineering of Sapienza University of Rome on research and support to Renewable Energy Communities.

Appendix A. Tables

Table A1
Natural gas price (c€/m3) based on consumption band and year.

	Annual consumption band (*1000 m^3)				
Year	< 26	26–260	260–2600	2600–26000	26000–104000
2014	78.88	62.19	43.11	35.12	33.33
2015	76.08	59.05	39.73	32.43	30.46
2016	69.84	52.90	34.40	27.50	25.75
2017	68.70	51.78	30.90	25.62	25.16
2018	71.63	54.16	34.10	29.05	28.78
2019	76.16	57.06	38.17	30.51	76.16
2020	73.19	52.49	33.80	25.68	22.97
2021	79.8	57.99	39.13	35.42	40.76
Average	74.29	55.95	36.67	30.17	35.42

Table A2
Purchasing and selling electricity prices in various time slots of the year. F1: 8–19 Mo-Fr. F2: 7–8 and 19–23 Mo-Fr and 7–23 Sa. F3: 23–7 Mo-Sa, all Sundays and holidays.

	Purchasing (€/kWh)			Selling (€/kWh)		
Month	F1	F2	F3	F1	F2	F3
Jan	0.08652	0.08364	0.068625	0.05996	0.0571	0.048093

(*continued on next page*)

Table A2 (*continued*)

Month	Purchasing (€/kWh)			Selling (€/kWh)		
	F1	F2	F3	F1	F2	F3
Feb	0.085585	0.08241	0.068843	0.054693	0.051233	0.044435
Mar	0.081268	0.08021	0.066493	0.046313	0.045508	0.03867
Apr	0.061615	0.065635	0.05433	0.04202	0.04067	0.03234
May	0.062363	0.065498	0.054418	0.04352	0.042898	0.03259
Jun	0.066145	0.067475	0.057408	0.04605	0.040398	0.03644
Jul	0.07978	0.075615	0.06432	0.052975	0.047268	0.039603
Aug	0.070375	0.071875	0.06009	0.0541	0.04975	0.043175
Sep	0.076425	0.074755	0.062415	0.055813	0.049225	0.044535
Oct	0.081188	0.08229	0.067915	0.054353	0.051125	0.044868
Nov	0.088668	0.085925	0.071115	0.061245	0.056583	0.04748
Dec	0.090878	0.088215	0.072735	0.065495	0.057763	0.046873

Table A3
Variable and objective function values of the optimal Pareto-front. The selected solution is highlighted in bold font.

Solution	PV capacity(kW)						Battery capacity (kWh)			Cogenerator size (kW)			Import from grid(kWh)	NPV(€)
	PV1	PV2	PV3	PV4	PV5	PV6	Batt1	Batt2	Batt3	Cog1	Cog2	Cog3	OF1	OF2
1	447	90	175	49	712	343	300	100	160	160	55	15	4725861	10589756
2	164	6.3	31.5	1.6	247	74	20	20	20	5	5	5	9382678	5264117
3	455	79	178	49	666	342	20	40	160	25	20	5	6494987	7033160
4	435	6.3	39.4	4.7	209	72.5	20	20	20	5	5	5	8993646	5434734
5	403	52	178	28	713	337	20	20	20	55	20	5	5982198	7497360
6	435	6.3	39.4	1.6	209	329	20	20	20	5	5	5	8583999	5613127
7	403	79	178	47	713	339	20	20	120	90	20	5	5478131	8249983
8	378	44	20.5	1.6	636	334	20	20	60	5	5	5	7943156	5927847
9	447	77	169	49	712	343	300	100	100	160	55	5	4870474	10335657
10	447	79	45.7	47	594	342	20	60	140	25	5	5	7168148	6536984
11	414	52	170	1.6	209	334	20	20	160	5	5	5	8316844	5812551
12	447	90	175	49	712	345	300	20	20	105	55	10	4940145	9411979
13	427	80	178	47	704	337	20	20	20	15	20	5	6765677	6743087
14	378	46	31.5	44	619	339	20	20	20	15	5	5	7600567	6163878
15	433	52	175	47	712	342	20	20	20	55	40	5	5720148	7907852
16	444	52	176	47	712	342	20	120	180	85	55	10	5159449	9000095
17	**446**	**88**	**176**	**49**	**712**	**345**	**300**	**20**	**20**	**105**	**55**	**10**	**4942702**	**9410641**
18	378	35	31.5	28	614	339	20	20	20	15	5	5	7651497	6139271
19	432	77	170	47	712	343	20	20	100	85	40	5	5298929	8536728
20	432	88	175	47	712	343	20	20	140	80	40	10	5235475	8589104

Appendix B. White certificate calculations

First, PES is calculated as [70]:

$$PES = \left(1 - \frac{1}{\frac{CHP\ H_\eta}{Ref\ H_\eta} + \frac{CHP\ E_\eta}{Ref\ E_\eta}}\right) * 100 \tag{7}$$

where $CHP\ H_\eta$ and $CHP\ E_\eta$ are the thermal and electrical efficiency of cogeneration units. $Ref\ H_\eta$ and $Ref\ E_\eta$ are the reference efficiency values for separate heat and separate electricity production. As reported in [70], values of $Ref\ H_\eta$ and $Ref\ E_\eta$ are equal to 90% and 52.5% correspondingly.

To receive the *White Certificates*, cogeneration units need to meet a minimum requirement and be categorized as high-efficiency cogenerators. The threshold of this minimum requirement is based on the PES index for different electricity capacities of cogeneration units as:

- PES>10% Electricity generation capacity > 1 MW
- PES>0% Electricity generation capacity < 1 MW

Subsequently, the amount of saved primary energy (*RISP*) is calculated as [71]:

$$RISP = \frac{E_{CHP}}{\eta_E RIF} + \frac{H_{CHP}}{\eta_T RIF} - F_{CHP} \tag{8}$$

in which E_{CHP} and H_{CHP} are the amounts of electrical and thermal output energy of cogenerators. F_{CHP} refers to the produced energy of the fuel. $\eta_T RIF$ and $\eta_E RIF$ are thermal and electrical average conventional efficiency with values of 90% and 46% respectively. Based on the primary energy savings calculated in Eq. (5), the cogeneration unit shall be entitled in the specific year to a number of *White Certificates (CB)* equal to:

$$CB = RISP*0.086*K \tag{9}$$

in which K is the "harmonization coefficient" and is a function of cogenerator electricity output as. K is formed from different portions based on the electricity output of the related cogeneration unit:

- K=1.4 for power quotes up to 1 MW_e
- K=1.3 for the portion of power between 1 MWe and 10 MW_e
- K=1.2 for the portion of power between 10 MWe and 80 MW_e
- K=1.1 for the portion of power between 80 MWe and 100 MW_e
- K=1.0 for the portion of power more than 100 MW_e

For example, if the co-generator produces 100 MWh that 80 MWh of it is considered in high-efficiency criterion, and if this unit has worked for 5000 h/year:

$$high_{eff}\ power = \frac{80,000}{5000} = 16MW = 1 + 9 + 6 \tag{10}$$

and K would be calculated as:

$$K = \frac{1.4*1 + 1.3*9 + 1.2*6}{16} = 1.269 \tag{11}$$

Finally, the value of each *White Certificate* or Energy Efficiency Certificate fluctuates between € 250 and € 260 [72].

Appendix C. Controller flowchart

Due to the complexity of the controller, only a small part of the details is shown in Fig. C1 where the algorithm starts from a negative surplus of block 0. The rest of the algorithm has similar flowcharts with minor details.

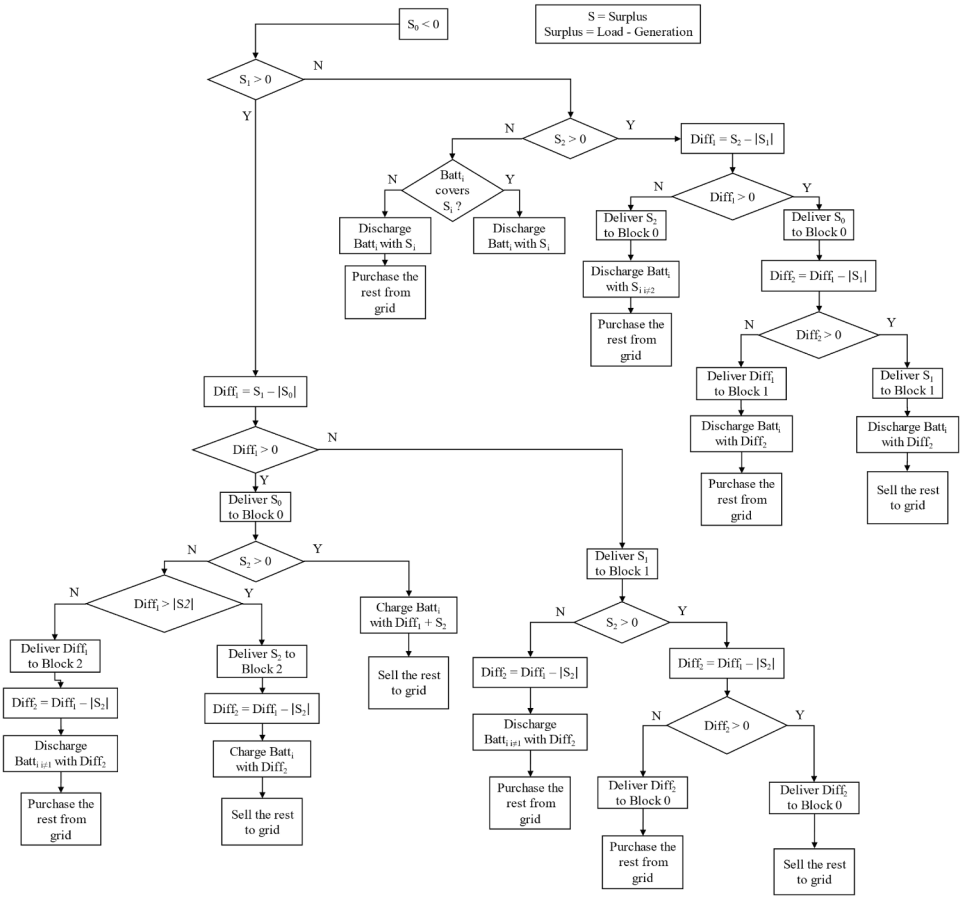

Fig. C1. A detailed portion of the controller starting with negative surplus of block 0.

Appendix D. Governing equations and technical data

PV panels:

The four-parameter equivalent circuit model [49] is module photocurrent at reference conditions ($I_{L,ref}$), diode reverse saturation current at reference conditions ($I_{o,ref}$), empirical PV curve-fitting parameter (γ), and module series resistance (R_S).

$$I = I_L - I_o\left[exp\left(\frac{q}{\gamma k T_c}(V + IR_S)\right) - 1\right] \tag{12}$$

where γ and R_S are constant parameters and I_L is a linear function of the solar irradiance:

$$I_L = I_{L,ref}\frac{G_T}{G_{T,ref}} \tag{13}$$

in which $G_{T,ref}$ is the reference solar irradiance and is equal to 1000 W/m^2. The technical specification of the PV model is adapted from FuturaSun FU 315 Monocrystalline PV Module [73].

Batteries:

This model represents a lead-acid battery that operates based on a simple energy balance [49] and the battery's state of charge over time is calculated based on charge and discharge rates. The energy balances are formulated as:

$$E_{ch} = \eta_{ch}\int_t^{t+1} P_{ch}dt \tag{14}$$

$$E_{disc} = \eta_{disc}\int_t^{t+1} P_{disc}dt \tag{15}$$

where *ch* and *disc* refer to the charge and discharge modes of the battery. η is the efficiency, E is the stored or discharged energy from the battery and P is the input power. The input power is controlled not to exceed P_{min} and P_{max}.

Cogenerators:

The output electric power (P_{el}) is calculated as:

$$P_{el} = (\eta_{\text{el}})(\rho_{\text{fuel}})\left(\dot{V}_{\text{fuel}}\right)(LHV_{\text{fuel}}) \tag{16}$$

where ρ, $\dot{V}$ and LHV are density, volumetric flow rate and low heating value of the fuel. The normalized power is required to obtain the fuel consumption from characteristic curves using:

$$P_{normalized} = \frac{P_{el}}{P_{rated}} \tag{17}$$

$$\dot{V}_{\text{fuel}} = a + bP_{normalized} \tag{18}$$

where a and b are constant reference values of fuel consumption curves (Table A.4). The electrical efficiency and the thermal output are calculated as:

$$\eta_{\text{el}} = \frac{P_{el}}{\dot{V}_{\text{fuel}}} \tag{19}$$

$$Q_{\text{th}} = P_{el}\frac{1-\eta_{\text{el}}}{\eta_{\text{el}}} \tag{20}$$

Table A4 delivers the technical data and input parameters of the implemented TRNSYS components with their corresponding values and units.

Table A4
Technical input parameters of energy unit models. Refer to Table 5 for each unit's capacity.

Parameter	Value	Unit
PV panel (Type 103)		
Module short-circuit current (ref. cond)	9.8	A
Module open-circuit voltage (ref. cond)	41.02	V
Reference cell temperature	25	°C
Reference insolation	1000	W/m^2
Module voltage at max power point and reference conditions	33.42	V
Module current at max power point and reference conditions	9.43	A
Temperature coefficient of short circuit current (ref. cond)	0.0344	A/K
Temperature coefficient of open circuit voltage (ref. cond)	−0.273	V/K
Number of cells wired in series	36	–
Module temperature at nominal operating cell temperature	40	°C

(*continued on next page*)

Table A4 (*continued*)

Parameter	Value	Unit
Array slope	36	degree
Active module area	0.89	m^2
Battery (Type 47)		
Cells in parallel	1	–
Cells in series	1	–
Charge/discharge efficiency	0.95	–
Cogenerator (Type 120)		
Fuel type	methane	–
Maximum allowable power	40 % of rated power	kW
Maximum allowable power	120 % of rated power	kW
First coefficient of fuel consumption curve [49]	2.078	l/h
Second coefficient of fuel consumption curve [49]	9.2521	l/h

References

[1] P. Office of the European Union, Clean energy for all Europeans Energy, doi: 10.2833/21366.

[2] S. Impram, S. Varbak Nese, B. Oral, Challenges of renewable energy penetration on power system flexibility: a survey, Sep. 01, 2020, Elsevier Ltd. doi: 10.1016/j.esr.2020.100539.

[3] H. Lund, B. Möller, B.V. Mathiesen, A. Dyrelund, The role of district heating in future renewable energy systems, Energy 35 (3) (2010) 1381–1390, https://doi.org/10.1016/j.energy.2009.11.023.

[4] S. Werner, District heating and cooling in Sweden, 2017, Elsevier Ltd. doi: 10.1016/j.energy.2017.03.052.

[5] S. Buffa, M. Cozzini, M. D'Antoni, M. Baratieri, R. Fedrizzi, 5th generation district heating and cooling systems: a review of existing cases in Europe, Apr. 01, 2019, *Elsevier Ltd. doi: 10.1016/j.rser.2018.12.059*.

[6] G. Krajačić, N. Duić, Z. Zmijarević, B. V. Mathiesen, A. A. Vučinić, and M. Da Graa Carvalho, Planning for a 100% independent energy system based on smart energy storage for integration of renewables and CO2 emissions reduction, Appl Therm Eng, vol. 31, no. 13, pp. 2073–2083, Sep. 2011, doi: 10.1016/j.applthermaleng.2011.03.014.

[7] M. Ghorab, Energy hubs optimization for smart energy network system to minimize economic and environmental impact at Canadian community, Appl. Therm. Eng. 151 (Mar. 2019) 214–230, https://doi.org/10.1016/j.applthermaleng.2019.01.107.

[8] L. Zhang, Y. Li, H. Zhang, X. Xu, Z. Yang, W. Xu, A review of the potential of district heating system in Northern China, Appl. Therm. Eng. 188 (Apr. 2021), https://doi.org/10.1016/j.applthermaleng.2021.116605.

[9] S.Y. Abujarad, M.W. Mustafa, J.J. Jamian, Recent approaches of unit commitment in the presence of intermittent renewable energy resources: a review, Apr. 01, 2017, Elsevier Ltd. doi: 10.1016/j.rser.2016.11.246.

[10] A. S. Brouwer, M. Van Den Broek, A. Seebregts, A. Faaij, Impacts of large-scale intermittent renewable energy sources on electricity systems, and how these can be modeled, 2014, Elsevier Ltd. doi: 10.1016/j.rser.2014.01.076.

[11] S. Vadi, S. Padmanaban, R. Bayindir, F. Blaabjerg, L. Mihet-Popa, A review on optimization and control methods used to provide transient stability in microgrids,"Sep. 19, 2019, MDPI AG. doi: 10.3390/en12183582.

[12] Q. Wang, et al., Analysis on the coupling characteristics of frequency stability and voltage stability in weak connected power grid with high ratio of clean energy, Energy Rep. 8 (Apr. 2022) 1432–1437, https://doi.org/10.1016/j.egyr.2021.11.118.

[13] B. Mohandes, M.S. El Moursi, N. Hatziargyriou, S. El Khatib, A review of power system flexibility with high penetration of renewables, IEEE Trans. Power Syst. 34 (4) (Jul. 2019) 3140–3155, https://doi.org/10.1109/TPWRS.2019.2897727.

[14] J. Sun, M. Wu, H. Jiang, X. Fan, T. Zhao, Advances in the design and fabrication of high-performance flow battery electrodes for renewable energy storage, May 26, 2021, Elsevier Ltd. doi: 10.1016/j.adapen.2021.100016.

[15] B. Diouf, R. Pode, Potential of lithium-ion batteries in renewable energy, Apr. 01, 2015, Elsevier Ltd. doi: 10.1016/j.renene.2014.11.058.

[16] L. Olatomiwa, S. Mekhilef, M.S. Ismail, M. Moghavvemi, Energy management strategies in hybrid renewable energy systems: a review, 2016, Elsevier Ltd. doi: 10.1016/j.rser.2016.05.040.

[17] S. Werner, International review of district heating and cooling, Oct. 15, 2017, Elsevier Ltd. doi: 10.1016/j.energy.2017.04.045.

[18] B. Rezaie, M.A. Rosen, District heating and cooling: review of technology and potential enhancements, Appl. Energy 93 (2012) 2–10, https://doi.org/10.1016/j.apenergy.2011.04.020.

[19] A. Kang, I. Korolija, D. Rovas, Photovoltaic thermal district heating: a review of the current status, opportunities and prospects," nov. 25, 2022, Elsevier Ltd. doi: 10.1016/j.applthermaleng.2022.119051.

[20] A. Behzadi, A. Arabkoohsar, Y. Yang, Optimization and dynamic techno-economic analysis of a novel PVT-based smart building energy system, Appl. Therm. Eng. 181 (Nov. 2020), https://doi.org/10.1016/j.applthermaleng.2020.115926.

[21] M. Rivarolo, A. Cuneo, A. Traverso, A.F. Massardo, Design optimisation of smart poly-generation energy districts through a model based approach, Appl. Therm. Eng. 99 (Apr. 2016) 291–301, https://doi.org/10.1016/j.applthermaleng.2015.12.108.

[22] M.A. Mirzaei, et al., Evaluating the impact of multi-carrier energy storage systems in optimal operation of integrated electricity, gas and district heating networks, Appl. Therm. Eng. 176 (Jul. 2020), https://doi.org/10.1016/j.applthermaleng.2020.115413.

[23] N. Good, E.A. Martínez Ceseña, P. Mancarella, Ten questions concerning smart districts, Build Environ 118 (2017) 362–376, doi: 10.1016/j.buildenv.2017.03.037.

[24] R.H. Lasseter, P. Paigi, "Microgrid: a conceptual solution", in: PESC Record - IEEE Annual Power Electronics Specialists Conference, 2004, pp. 4285–4290, https://doi.org/10.1109/PESC.2004.1354758.

[25] V. Kaisermayer, et al., Smart control of interconnected district heating networks on the example of '100% Renewable District Heating Leibnitz', Smart Energy 6 (May 2022) https://doi.org/10.1016/j.segy.2022.100069.

[26] M.F. Akorede, H. Hizam, E. Pouresmaeil, "Distributed energy resources and benefits to the environment," Feb. 2010. doi: 10.1016/j.rser.2009.10.025.

[27] C. Klemm, P. Vennemann, "Modeling and optimization of multi-energy systems in mixed-use districts: a review of existing methods and approaches," Jan. 01, 2021, Elsevier Ltd. doi: 10.1016/j.rser.2020.110206.

[28] N.H. Afgan, M.G. Carvalho, Sustainability assessment of a hybrid energy system, Energy Policy 36 (8) (2008) 2903–2910, https://doi.org/10.1016/j.enpol.2008.03.040.

[29] G. Comodi, M. Lorenzetti, D. Salvi, A. Arteconi, Criticalities of district heating in Southern Europe: lesson learned from a CHP-DH in Central Italy, Appl. Therm. Eng. 112 (Feb. 2017) 649–659, https://doi.org/10.1016/j.applthermaleng.2016.09.149.

[30] C. Widmann, D. Lödige, A. Toradmal, B. Thomas, Enabling CHP units for electricity production on demand by smart management of the thermal energy storage, Appl. Therm. Eng. 114 (2017) 1487–1497, https://doi.org/10.1016/j.applthermaleng.2016.08.065.

[31] H.H. Erdem, et al., Thermodynamic analysis of an existing coal-fired power plant for district heating/cooling application, Appl. Therm. Eng. 30 (2–3) (Feb. 2010) 181–187, https://doi.org/10.1016/j.applthermaleng.2009.08.003.

[32] S. Upadhyay, M.P. Sharma, A review on configurations, control and sizing methodologies of hybrid energy systems, Elsevier Ltd., 2014, https://doi.org/10.1016/j.rser.2014.05.057.

[33] J. Salpakari, P. Lund, Optimal and rule-based control strategies for energy flexibility in buildings with PV, Appl. Energy 161 (Jan. 2016) 425–436, https://doi.org/10.1016/j.apenergy.2015.10.036.

[34] J. De Hoog, K. Abdulla, R. R. Kolluri, P. Karki, Scheduling fast local rule-Based controllers for optimal operation of energy storage, in: e-Energy 2018 - Proceedings of the 9th ACM International Conference on Future Energy Systems, Association for Computing Machinery, Inc, Jun. 2018, pp. 168–172. doi: 10.1145/3208903.3208917.

[35] J. Liu, S. Cao, X. Chen, H. Yang, J. Peng, Energy planning of renewable applications in high-rise residential buildings integrating battery and hydrogen vehicle storage, Appl. Energy 281 (Jan. 2021), https://doi.org/10.1016/j.apenergy.2020.116038.

[36] I. Prodan, E. Zio, A model predictive control framework for reliable microgrid energy management, Int. J. Electr. Power Energy Syst. 61 (2014) 399–409, https://doi.org/10.1016/j.ijepes.2014.03.017.

[37] A. Bolzoni, A. Parisio, R. Todd, A. Forsyth, Model predictive control for optimizing the flexibility of sustainable energy assets: an experimental case study, Int. J. Electr. Power Energy Syst. 129 (Jul. 2021), https://doi.org/10.1016/j.ijepes.2021.106822.

[38] T.M. Kneiske, M. Braun, D.I. Hidalgo-Rodriguez, A new combined control algorithm for PV-CHP hybrid systems, Appl. Energy 210 (Jan. 2018) 964–973, https://doi.org/10.1016/j.apenergy.2017.06.047.
[39] M.D.A. Al-falahi, S.D.G. Jayasinghe, H. Enshaei, A review on recent size optimization methodologies for standalone solar and wind hybrid renewable energy system, 2017, Elsevier Ltd. doi: 10.1016/j.enconman.2017.04.019.
[40] J. Li, Optimal sizing of grid-connected photovoltaic battery systems for residential houses in Australia, Renew. Energy 136 (Jun. 2019) 1245–1254, https://doi.org/10.1016/j.renene.2018.09.099.
[41] H. Bahlawan, M. Morini, M. Pinelli, P.R. Spina, M. Venturini, Optimization of energy and economic scheduling of a hybrid energy plant by using a dynamic programming approach, Appl. Therm. Eng. 187 (2021), https://doi.org/10.1016/j.applthermaleng.2021.116577.
[42] Y. Xu, C. Yan, H. Liu, J. Wang, Z. Yang, Y. Jiang, Smart energy systems: A critical review on design and operation optimization, Nov. 01, 2020, Elsevier Ltd. doi: 10.1016/j.scs.2020.102369.
[43] A.L. Bukar, C.W. Tan, A review on stand-alone photovoltaic-wind energy system with fuel cell: system optimization and energy management strategy, Jun. 01, 2019, Elsevier Ltd. doi: 10.1016/j.jclepro.2019.02.228.
[44] A. Awad, P. Bazan, R. German, Optimized operation of PV/T and micro-CHP hybrid power systems, Technol. Econ. Smart Grids Sustain. Energy 1 (1) (Dec. 2016), https://doi.org/10.1007/s40866-016-0004-3.
[45] B. Zhao, X. Zhang, P. Li, K. Wang, M. Xue, C. Wang, Optimal sizing, operating strategy and operational experience of a stand-alone microgrid on Dongfushan Island, 2014, Elsevier Ltd. doi: 10.1016/j.apenergy.2013.09.015.
[46] T. Schütz, et al., Optimal design of energy conversion units for residential buildings considering German market conditions, Energy 139 (2017) 895–915, https://doi.org/10.1016/j.energy.2017.08.024.
[47] D. Zhang, et al., Research on the configuration and operation effect of the hybrid solar-wind-battery power generation system based on NSGA-II, Energy 189 (Dec. 2019), https://doi.org/10.1016/j.energy.2019.116121.
[48] K. Deb, A. Pratap, S. Agarwal, T. Meyarivan, A fast and elitist multiobjective genetic algorithm: NSGA-II, IEEE Trans. Evol. Comput. 6 (2) (Apr. 2002) 182–197, https://doi.org/10.1109/4235.996017.
[49] University of Wisconsin–Madison. Solar Energy Laboratory., "TRNSYS, a Transient Simulation Program.," 1975, *Madison, Wis. :The Laboratory,*.
[50] "Update of ASHRAE Standard 140 Section 5.2 and Related Sections (BESTEST Building Thermal Fabric Test Cases) Energy Systems Division." [Online]. Available: www.anl.gov.
[51] K. Kanyarusoke, J. Gryzagoridis, G. Oliver, Validation of TRNSYS modelling for a fixed slope photovoltaic panel, Turk. J. Electr. Eng. Comput. Sci. 24 (6) (2016) 4763–4772, https://doi.org/10.3906/elk-1502-38.
[52] D. Firmanda, A. Riza, S. Ihtsham-Ul, and H. Gilani, "Standalone Photovoltaic System Sizing using Peak Sun Hour Method and Evaluation by TRNSYS Simulation," 2014.
[53] I.B. Mansir, E.H. Bani Hani, N. Farouk, A. AlArjani, H. Ayed, D.D. Nguyen, Comparative transient simulation of a renewable energy system with hydrogen and battery energy storage for residential applications, Int. J. Hydrogen Energy 47 (62) (Jul. 2022) 26198–26208, https://doi.org/10.1016/j.ijhydene.2022.02.092.
[54] A. Rana, G. Gróf, Assessment of prosumer-based energy system for rural areas by using TRNSYS software, Cleaner Energy Systems 8 (Aug. 2024), https://doi.org/10.1016/j.cles.2024.100110.
[55] P.J. Axaopoulos, E.D. Fylladitakis, K. Gkarakis, Accuracy analysis of software for the estimation and planning of photovoltaic installations, Int. J. Energy Environ. Eng. 5 (1) (Apr. 2014) 1–8, https://doi.org/10.1007/s40095-014-0071-y.
[56] Meteonorm V5, "http://www.meteonorm.com.".
[57] Meteotest, "http://www.meteotest.com.".
[58] N.B. M., M.K. Bernier, "Calling Python from TRNSYS with CFFI," 2022.
[59] J. Blank, K. Deb, Pymoo: multi-objective optimization in python, IEEE Access 8 (2020) 89497–89509, https://doi.org/10.1109/ACCESS.2020.2990567.
[60] National Renewable Energy Laboratory, "https://atb.nrel.gov/electricity/2021/utility-scale_pv.".
[61] K. Mongird *et al.*, "Energy Storage Technology and Cost Characterization Report," 2019.
[62] U. States Department of Energy, "Combined Heat and Power Technology Fact Sheet Series ADVANCED MANUFACTURING OFFICE.".
[63] ARERA, "https://www.arera.it/it/dati/gpcfr2.htm.".
[64] ARERA, "https://www.arera.it/it/prezzi.htm.".
[65] GSE, "https://www.gse.it/servizi-per-te/fotovoltaico/ritiro-dedicato/documenti.".
[66] A. Panichella, An adaptive evolutionary algorithm based on non-euclidean geometry for many-objective optimization, in: GECCO 2019 - Proceedings of the 2019 Genetic and Evolutionary Computation Conference, Association for Computing Machinery, Inc, Jul. 2019, pp. 595–603. doi: 10.1145/3321707.3321839.
[67] E. Zitzler, L. Thiele, Multiobjective Optimization Using Evolutionary Algorithms A Comparative Case Study.
[68] A.P. Wierzbicki, A mathematical basis for satisficing decision making, 1982.
[69] "LINEE GUIDA alla presentazione dei progetti per il Programma per la Riqualificazione Energetica degli edifici della Pubblica Amministrazione Centrale PREPAC (D.M. 16 Settembre 2016)," 2017.
[70] Criteri espressi all'interno del DM 4 agosto 2011, "https://www.mise.gov.it/images/stories/normativa/DM-4-AGOSTO-2011-2.pdf.".
[71] GSE, "Guida alla Cogenerazione ad Alto Rendimento CAR, Edizione n.1.".
[72] "Decreto Interministeriale 11 gennaio 2018.".
[73] "FuturaSun FU 315 M," https://www.enfsolar.com/pv/panel-datasheet/crystalline/43640. Accessed at 12.05.2022.